Journal of the Technical University of Gabrovo

https://mc04.manuscriptcentral.com/jtug

POROSITY DISTRIBUTION AND MICROHARDNESS OF A COLD ARC PULSE™ WIRE ARC ADDITIVELY MANUFACTURED AlSi$_x$ MECHANICAL PLATE

Nikolay Petrov[1], Maria Ormanova[2]*, Iliya Zhelezarov[1]

[1]*Technical University of Gabrovo, 5300 Gabrovo, Bulgaria*

[2]*Institute of Electronics of Bulgarian Academy of Sciences, 1784 Sofia, Bulgaria*

ARTICLE INFO

Article history:
Received 11 April 2024
Accepted 13 May 2024

Keywords:
AlSi5; structure; porosity; microhardness

http://doi.org/10.62853/HAEA7843

ABSTRACT

Porosity is known as the main problem of aluminum alloys regardless of the method for formation of aluminum components due to the unique thermophysical properties of this metal. The larger the heat input is, the higher the likelihood is of formation of pores within the structure of the components, whether be they caused by the gas adsorption or due to the expansion and then shrinkage of the material during the heating/cooling cycle. Since the pore formation mechanisms of additively manufactured specimens is still unclear, during the present work a wire arc additively manufactured specimen was used in order to study the concentration of pores within the structure of the last along its volume. Additionally, the less studied cold arc pulse (CAP) mode was employed during the specimens manufacturing. Since the structure directly influences the mechanical properties of the components, a microhardness map was prepared as well as investigation of the microhardness as a function of the specimen's height. The results were summarized and indicated an increasing trend of the porosity of the specimen towards its top section. The larger defects were observed closer towards the bottom of the specimen due to the lower interpass temperature, this the worse fusion of the aluminum. Despite this the microhardness along the face-wall of the specimen and its cross section remained the same within the margin of error. The possibility of decreasing the porosity and increasing the quality of the deposited components was discussed.

1. INTRODUCTION

Additive manufacturing systems have been developed in recent years to investigate the possibility for direct manufacturing of metallic components with minimal production losses compared to conventional production techniques [1]. This is determined by a number of factors. The main one is the capability of additive manufacturing systems to make near ready components that require minimal to none mechanical treatment prior to their implementation in the industry [2]. Another factor that is partially ecologically friendly is the reusability of waste materials that form while producing metallic components using traditional methods. Those byproducts can be easily reformed and reused again for the production of metallic components [3]. Additionally, a natural occurrence during the operation of every factory is the decommissioning of high-class equipment which results in temporary losses for the company. The decommissioned instruments such as robotic arms, welding machines and more can be repurposed and reorganized as additive manufacturing systems with minimal investments.

Considering the above mentioned reasons for the development of additive manufacturing systems the most common ones, which require the least investments are the ones that use the so called direct energy deposition (DED) approach. Those systems are based on using lasers and electric arcs as heat sources [4]. The cheapest and easiest to integrate systems for DED are the wire arc additive manufacturing (WAAM) ones in order to consolidate the efficiency of production. Although WAAM has some notable disadvantages compared to methods employing laser deposition methods such as low precision of deposition and lower efficiency [5, 6], it also has some standout advantages such as a high deposition rate and a high-volume production (superb production of large components) [7].

Wire arc additive manufacturing can be performed by employing different techniques, the most common out of which is gas metal arc welding (GMAW). This is the preferred technique over others due to the simplicity and low cost of the technical equipment required for realization of this manufacturing method. In addition, the GMAW technique itself can be performed in different working modes which vary by the way the welding wire is integrated in the welded structure. The most common mode employed by researchers worldwide is the cold metal transfer (CMT) one due to the low heat input which is of high importance when aluminum alloys are concerned [8]. As it is known aluminum and its alloy are highly susceptible to the formation of defects such as pores and

* Corresponding author. E-mail: maria.ormanova87@gmail.com

cracks. The low heat input of the CMT mode leads to the manufacturing of low-defect aluminum structures with excellent mechanical properties [9]. The CMT mode uses a welding machine combined with a power supply specifically designed for welding, and a wire feeder. Once the arc is ignited the material is integrated in the locally molten zone of the specimen by moving the electrode backwards mechanically using the wire rollers. Another mode which can be used for manufacturing aluminum specimens, which also is characterized with a low heat input, is the cold arc pulse (CAP) one. Comparatively the two modes are almost identical with the primary difference between them being that the CAP mode utilizes high frequency switching in combination with the naturally occurring axial and radial forces that form between the weld bead and the electrode for bead separation. Since both modes can utilize the employment of a pulsing electric arc as a heat source the resultant heat input is lower compared to the heat input of conventional GMAW [10].

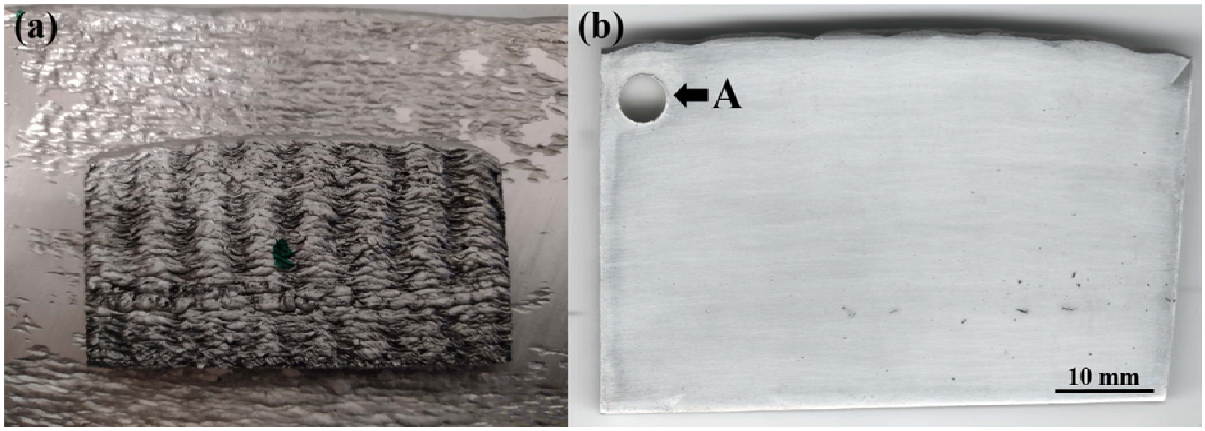

Fig. 1. Images of the (a) as deposited specimen, and (b) the same after polishing and etching

The production of aluminum components is of high importance for the industry due to the exceptionally high application of aluminum in practice [11]. The most common occurring fault when attempting to form aluminum based components is the formation of microscopic pores and cracks due to the high thermal gradient explained by the high temperature of the electric arc and the low temperature of the surrounding environment, accelerated by the high thermal conductivity of aluminum and its alloys [12]. Despite the previous attempts to study and modulate the porosity of CMT made specimens [13] unsatisfactory number of research is present regarding the porosity formation and characterization while building components in the CAP mode.

For this reason, the current research aims to provide general knowledge on the porosity formation during the cold arc pulse mode of WAAM of a AlSi5 specimen, and also provide some correlation between the formed structure and the resultant microhardness across the volume of the specimen.

2. EXPERIMENTAL PART

A wall-shaped specimen with dimensions of 70 x 40 x 6 mm was manufactured using a wire arc additive manufacturing setup consisting of a KUKA KR15 robot and an EWM Alpha Q552 welding machine. The method used for the deposition of the obtained sample was gas metal arc welding (GMAW) in the cold arc pulse (CAP) mode. The welding wire used for the experiments was a 1.2 mm in diameter made out of a silumin alloy AlSi5. The voltage of the electric arc was kept a constant at 16.5 V, while the current was 119 A. The wait time between the interlayers was 30 seconds in all cases. The movement of the torch in the direction of build-up of the specimen after every consecutive layer was 1.0 mm. The wire feeding rate was 100 mm/s, and the welding speed was 16 mm/s. The heat input Q (J/mm) was calculated in agreement with the MIG/MAG heat input formula given in [14] and was estimated to be 98 J/mm.

Figure 1a depicts an image of the as built specimen, and figure 1b depict the polished and etched surface of the specimen. The polishing procedure was done in a number of steps. Initially the sample was ground using a P240 grit abrasive paper, followed by P400, P800, P1000, and finally P2500. The surface of the sample was then etched using a 10 % HF acid solution. The orifice marked in figure 1b as “A” corresponds to an opening in the mechanical plate used for carrying out the porosity measurements using the Archimedes method described below.

The surface topography of the obtained specimen was studied initially using an optical microscope Drawell MIT 300/500. The size of the observed pores was determined using a specialized imaging software conjoined with the optical microscope.

The possible porosity formation was determined in agreement with the Archimedes method described in detail by Terris et al. [15]. For the purpose of this experiment two measurements are performed. One in open air as seen in figure 2a, where the density of the surrounding air was assumed to be $\rho = 0.0013$ gcm^{-3}, and one in a known density fluid as seen in figure 2b, which in this case was distilled water with a density of $\rho = 0.9982$ gcm^{-3}. According to popular theory in case any internal volumes of the samples are present, whether be they gas filled or hollow, the mass of the specimen in air and in a fluid should be different. This difference in mass can be used to calculate the density of the obtained specimen using equation (1).

$$\rho_s = \frac{M_a}{M_a - M_f}\left(\rho_f - \rho_a\right) + \rho_a \quad (1)$$

The density of the specimen ρ_s [gcm^{-3}] is proportional to its mass in air M_a [g], its mass in the fluid M_f [g], and the

density of the fluid ρ_f [gcm^{-3}] and the density of the air ρ_a [gcm^{-3}].

Once the density of the specimen is established its porosity is calculated using equation (2). The porosity [%] of the specimen is determined by the difference between its measured density ρ_m [gcm^{-3}] and the theoretical one for the selected material ρ_{th} [gcm^{-3}], which in the case of aluminum was assumed to be 2.7 gcm^{-3}.

$$\%\ porosity = 100 - \left(\frac{\rho_m * 100}{\rho_{th}} \right) \quad (2)$$

The formed structure of the specimen and the presence of defects within it such as micro-pores, cracks or others were studied using scanning electron microscopy (SEM) using both secondary and back-scattered electrons. Energy-dispersive X-ray spectroscopy (EDX) was also employed in order to differentiate the chemical components included within the AlSi5 alloy.

The microhardness of the specimen was studied using a Vickers hardness indenter ZwickRoell DuraScan G5. All measurements were taken using a load of 1 N corresponding to a weight of 100 grams. Each measurement was performed for a time of 5 seconds, and the distance between each indenter print was kept above three times the diameter of the print in agreement with the ISO-6507-1 standard for microhardness measurements.

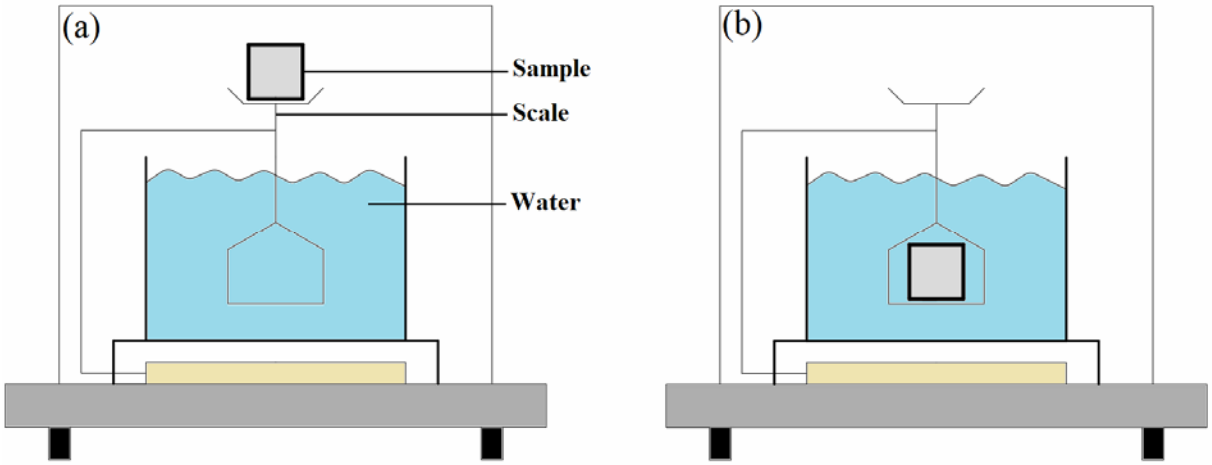

Fig. 2. Schematic of the Archimedes method: (a) measuring in air, and (b) measuring in water

3. RESULTS AND DISCUSSION

The manufactured component is shown in figure 1a. Evidently, using the current technological conditions of layer deposition a highly wavy outside layer was formed on both sides of the specimen. The formation of column-like structures on the side of the specimen indicates that either the pulse rate was too low for manufacturing a component with an even and smooth surface or the welding speed was too high. The grinding and etching procedures revealed a high quantity of pores in the structure of the specimen along its entire volume. A few larger cracks were also observed closer towards the bottom of the specimen. The uneven pattern at the bottom of the specimen hinted that the deposition temperature was too low and the fusion between the electrode material and the specimen was too low. With the increase of the height of the specimen this trend seized and an even structure was formed with improved fusion.

The results of the optical microscopy studies are shown in figure 3. The top section shown in figure 3a, the middle section is shown in figure 3b, and the bottom section is shown in figure 3c were studied separately due to the previously discussed change in the thermal fields during the process of WAAM, which could lead to structural changes in the specimen. Indeed, the bottom section of the specimen characterizes with a high concentration of micro sized pores where the maximum detected size of the pores in that region was 29.2 μm in diameter. Following the build-up direction, the size and concentration of the pores increases. At the middle of the specimen the largest detected pore had a diameter of 45.2 μm. The largest pore was detected at the top section of the specimen having a diameter of 135.9 μm. Comparatively the pores detected at the top section do not only have the highest concentration, but also the largest average size. The hypothesis for the formation of such large spherical-shaped pores within the structure of the specimen is the adsorption of gases from the surrounding air. Since oxygen and nitrogen both form oxide and nitride based bonds with the aluminum crystals they remain at the surface of the component. This means that the largest contributor to the formation of pores within the volume of the component is the adsorption of hydrogen specifically [16]. The increase in the concentration of pores is attributed to the natural diffusion processes that occur during the molten phase of the welded aluminum alloy which follow the direction of build-up. During the welding process a partial re-melting of the previously applied layer occurs which releases any trapped gases from the structure of the specimen. This is why the gas cavities concentration follows the direction of specimen manufacturing. Additionally, the highest concentration of pores is also attributed to the localized adsorption of hydrogen in the zone of the last deposited layer. A proven fact is that the increase of the temperature, thus the interpass temperature, leads to the increase of the solubility of hydrogen in the structure aluminum and its alloys [17]. This also hinders the formation of a high density pore-less structure. The natural diffusion processes that occur during the molten phase of the material are highly dependent on the solidification speed of the material as proven by [18]. This means that the longer the life of the melt pool is the better the diffusion of gases is. Evidently, the used welding speed is too high leading to a too high solidification speed, which hinders the diffusion of gases.

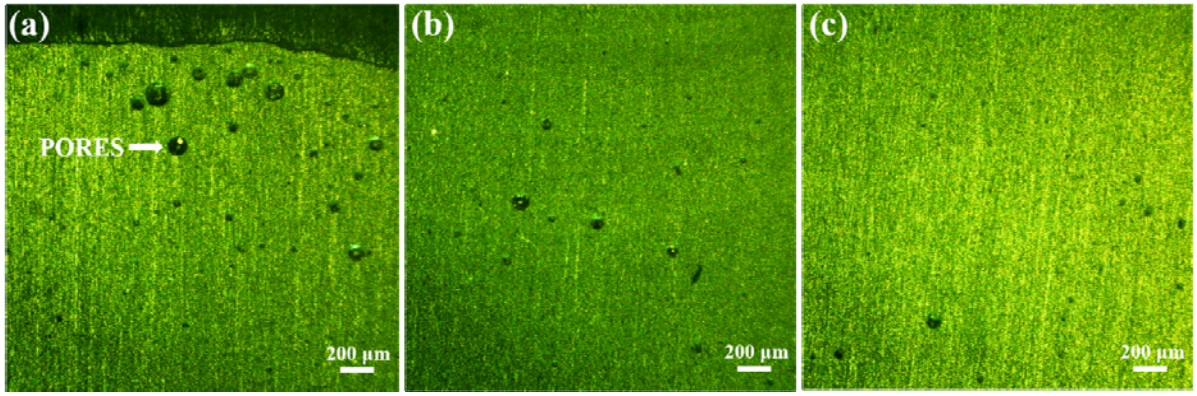

Fig. 3. Optical images of the top (a), middle (b), and bottom (c) sections of the specimens

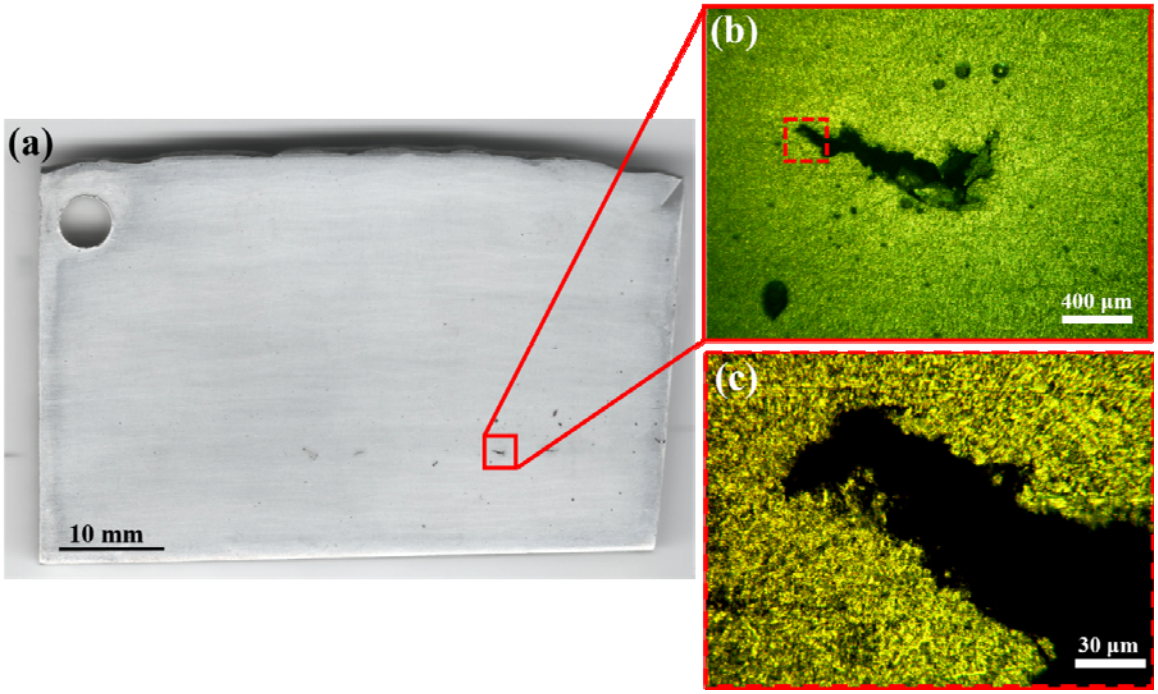

Fig.4. Optical images of the (a) polished specimen, (b) a large crack within its structure, and (c) a zoomed image of the formed crack

As mentioned above the presence of low density cavities (defects) was also studied in bulk using the Archimedes method. Three different measurements were performed in identical conditions. The results show that the density of the specimen ρ_s is ρ_{s1} = 2.59 gcm^{-3}, ρ_{s2} = 2.62 gcm^{-3}, and ρ_{s3} = 2.54 gcm^{-3}. The average density of the specimen was estimated to be ρ_s = 2.58 gcm^{-3}, which is slightly lower compared to the standard value for aluminum silicon alloys. Taking the present data into account the following levels of porosity were established corresponding to the three density measurements: %porosity = 4.4 %; %porosity = 3.3 %; %porosity = 6.3 %. The average porosity of the specimens was determined to be %porosity = 4.67 %. According to the measured dimensions of the specimen its volume is 13.65 cm^3. If 4.67 % account for defects present in the structure of the specimen such as gas pores, solidification pores, cracks, and others, then the approximate volume they take up in the specimen is about 0.637 cm^3.

Figure 4a shows an image previously displayed of the polished specimen. As it can be seen amidst its structure the presence of a large quantity of large cracks can be observed closer towards its bottom section. Figure 4b shows an image of the largest detected crack with a length of approximately 1300 µm. A zoomed image of the edge of the crack is shown in figure 4c. A number of micro-sized pores can also be observed close to the crack's vicinity. The concentration of cracks in the structure of the specimen decreases with the increase of its height.

The formation of a second type of defects in the structure of WAAM built specimens is in the form of irregularly shaped micro-pores. They are most commonly related to the rapid expansion of aluminum during the welding process and its subsequent compression during the process of cooling [19]. Since aluminum has one of the highest thermal expansion coefficients amongst other metals the difference in the volume of the material during its molten phase and its solid state is extremely substantial. The so-called solidification pores are detected in both cases using SEM while observing the upper section of the specimen as shown in figures 5a, and 5b. Similarly, solidification pores were also detected while studying the lower section of the specimen depicted in figures 5c and 5d. A slightly lower concentration of micro-sized pores was

estimated at the bottom of the specimen, which correlates to the slightly higher Vickers hardness in that area. The SEM images depicted in figure 5b and 5d both indicate the presence of αAl + Si eutectic structures dispersed in the primary αAl solid solution. In the case of the upper section of the specimen, the secondary eutectic structure is much more pronounced compared to that at the bottom.

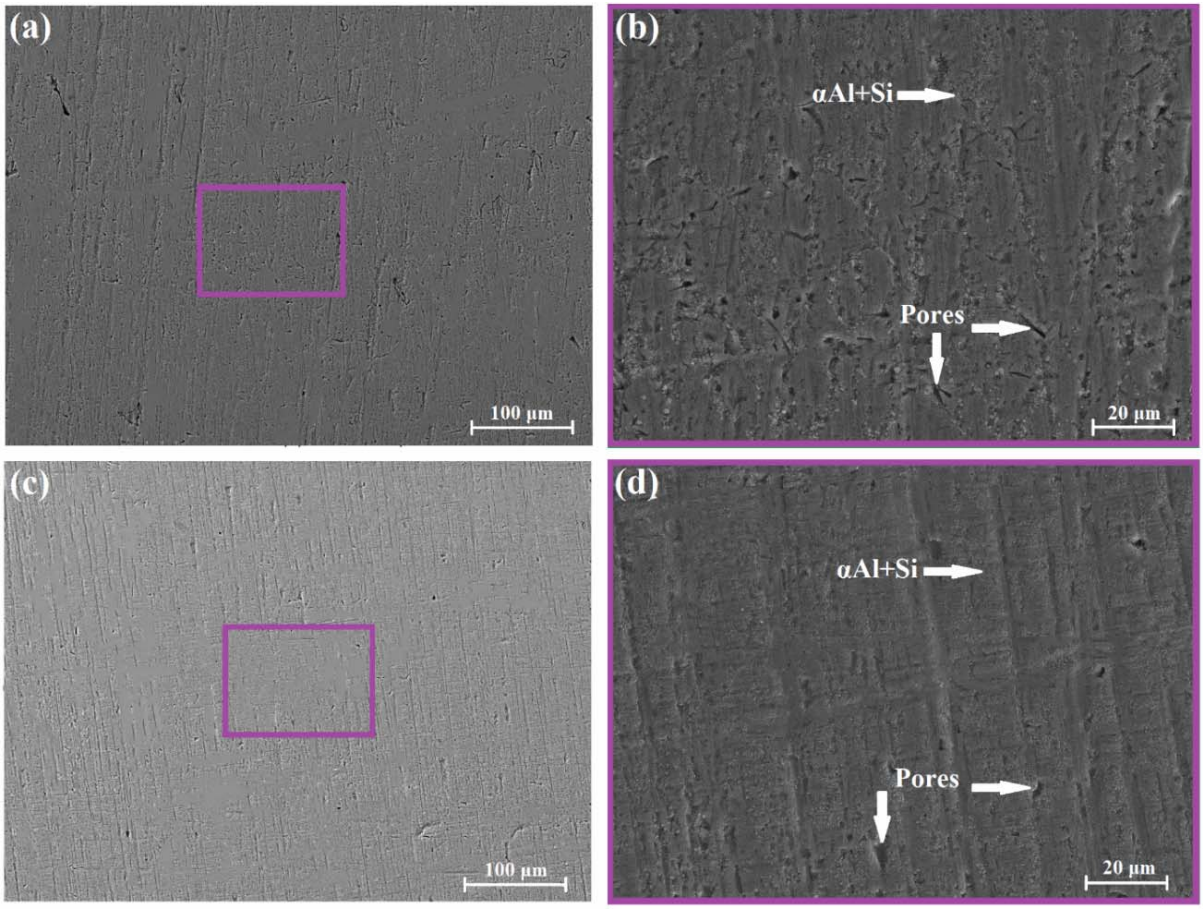

Fig. 5. SEM images from the upper part of the specimen at 500x zoom (a), and at 2000x zoom (b), and SEM images from the lower part of the specimen at 500x (c), and at 2000x zoom (d)

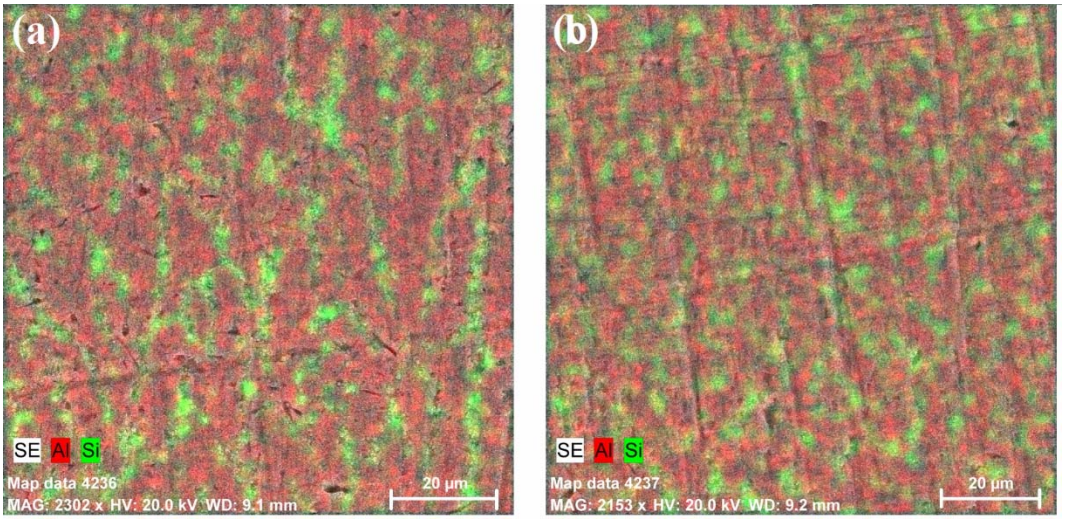

Fig. 6. EDX image from the upper part of the specimen (a), and EDX image from the lower part of the specimen (b)

In order to prove whether there is a real change in the secondary Si phase located in the αAl + Si eutectic formation the chemical composition of the samples was studied using EDX. A composition map was obtained where the separate elements are indicated in different colors. The Si eutectic structures are shown in green, and the αAl solid solution is shown in red. The results regarding the upper section of the specimen are shown in figures 6a.

In that area the concentration of the Si structures is 5.18 wt%. The results regarding the lower section of the specimen are shown in figures 6b. In that case the concentration of the Si structures is slightly lower – 4.87 wt%. The decrease of the concentration of the Si eutectics indicates that a shorter life of the melt pool was achieved at the lower section of the specimen which hindered the formation of the silicon-based eutectic structure.

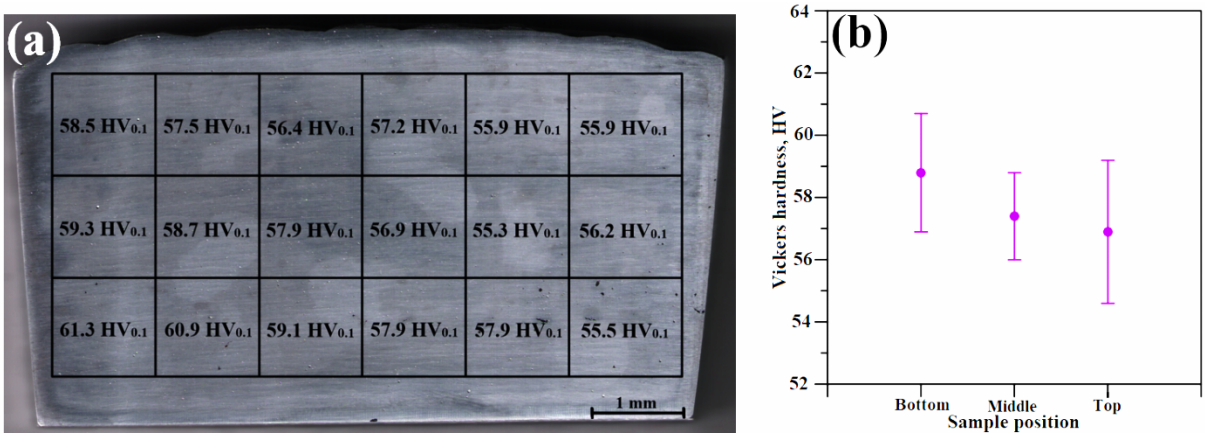

Fig. 7. Microhardness distribution along the entire volume of the specimen (a) and following the direction of build-up (b)

Studying the microhardness of the specimen led to the formation of the microhardness map shown in figure 7a. The lowest obtained measurement was 55.3 $HV_{0.1}$, and the highest one was 61.3 $HV_{0.1}$. The average calculated hardness of the specimen was 58.3 ±6 $HV_{0.1}$. As it is known due to the dynamic nature of the process of WAAM which leads to the formation of different thermal fields during the build-up process a change in the structure and therefore mechanical properties of the formed component can be observed following its height [20]. For this reason, the microhardness at the bottom, middle, and top sections of the specimen was studied and the results were compared as shown in figure 7b. Obviously a small decrease of the microhardness of the specimen at its top section was noticed in comparison tothe bottom one, however, the difference is miniscule within the margin of error. The reason for this slight decrease is the slightly higher concentration of pores at the top section of the specimen, which influence the results of the measurements. The average microhardness of the specimen is slightly lower compared to that reported by other researchers, which can once again be explained by the high concentration of defects [20].

4. CONCLUSION

In the process of studying a cold arc pulse mode wire arc additively manufactured AlSi5 specimen the following conclusions were drawn:

1. During the process of welding a high quantity of spherical-shaped pores were formed related to gaseous inclusions, indicating that the welding speed used in this process is too high;

2. A number of irregularly shaped solidification pores was observed in the structure of the specimen along the lower part of the specimen. Due to the increased interpass temperature the concentration increased towards the top of the specimen;

3. Due to the high concentration of defects in the structure of the specimen a substantial portion of its volume is taken up by low density cavities;

4. The secondary eutectic Si structure was not formed properly due to the shorter life of the melt pool at the lower section of the specimen compared to the top one;

5. Due to the longer life of the melt pool with the increase of the height of the specimen the Si particles formed Si cluster much more successfully, which resulted in higher expansion/shrinkage of the aluminum solid solution;

6. The increased concentration of defects due to the different thermal regime led to a slight worsening of the microhardness of the specimen, however, the values were nearly identical, within the margin of error indicating that the variation of the macro- and micro- pores concentration is of less importance to that mechanical parameter.

The performed study gives a basic insight on the formation of pores in cold arc pulse WAAM specimens and their influence on the microhardness of the specimens. The results prove the weak relationship between the concentration of pores and the microhardness of WAAM built specimens.

ACKNOWLEDGMENTS

The financial support of the Bulgarian National Science Fund, project #KP06-DO02/1 (2019) is highly appreciated.

REFERENCES

[1] Terris T., Andreau O., Peyre P., Adamski F., Koutiri I., Gorny C., Dupuy C. Optimization and comparison of porosity rate measurement methods of Selective Laster Melted metallic parts. Additive Manufacturing 28 (2019) 802-813

[2] Kotlarski G., Ormanova M., Ossenbrink R., Nikitin A., Doynov N., Valkov S., Michailov V. Fabrication and Characterization of Wire Arc Additively Manufactured AlSi5 Structures. Metalls 12 (2022) 1870

[3] Tawfik M., Nemat-Alla M., Dewidar M. Enhancing the properties of aluminum alloys fabricated using wire + arc additive manufacturing technique – A review. Journal of Materials Research and Technology 13 (2021) 754-768

[4] Prakash K., Nancharaih T., Rao V. Additive Manufacturing Techniques in Manufacturing – An Overview. Materials Today: Proceedings 5 (2018) 3873-3882

[5] Huang S., Liu P., Mokasdar A., Hou L. Additive manufacturing and its societal impact: a literature review.

International Journal of Advanced Manufacturing Technology 67 (2013) 1191-1203

[6] Frazier W. Metal Additive Manufacturing: A Review. Journal of Materials Engineering and Performance 23 (2014) 1917-1928

[7] Bikas H., Stavropoulos P., Chryssolouris G. Additive manufacturing methods and modelling approaches: a critical review. International Journal of Advanced Manufacturing Technology 83 (2015) 389-405

[8] Singh S., Ramakrishna S., Singh R. Material issues in additive manufacturing: A review. Journal of Manufacturing Processes 25 (2017) 185-200

[9] Ngo T., Kashani A., Imbalzano G., Nguyen K., Hui D. Additive manufacturing (3D printing): A review of materials, methods, applications and challenges. Composites Part B 143 (2018) 172-196

[10] Aldalur E., Suarez A., Veiga E., Holgado I., Ortega N. Tomography analysis of Al-Mg alloys manufactured by wire-arc directed energy deposition with different metal transfer modes. Alexandria Engineering Journal 82 (2023) 168-177

[11] Selvi S., Vishvaksenan A., Rajasekar E. Cold metal transfer (CMT) technology – An overview. Defence Technology 14 (2018) 28-44

[12] Wieczorowski M., Pereira A., Carou D., Gapinski B., Ramirez I. Characterization of 5356 Aluminum Walls Produced by Wire Arc Additive Manufacturing (WAAM). Materials 16 (2023) 2570

[13] Stojanovic B., Bukvic M., Epler I. Application of aluminum and aluminum alloys in engineering. Applied Engineering Letters 3 (2018) 52-62

[14] Kotlarski G., Ormanova M., Nikitin A., Morozova I., Ossenbrink R., Michailov V., Doynov N., Valkov S. Microstructural and Mechanical Properties of CAP-WAAM Single-Track Al5356 Specimens of Differing Scale. Machines 12 (2024) 72

[15] Köhler M., Hensel J., Dilger K. Effects of Thermal Cycling on Wire and Arc Additively Manufacturing of Al-5356 Components. Metals 10 (2020) 952

[16] Hauser T., Reisch R., Breese P., Lutz B., Pantano M., Nalam Y., Bela K., Kamps T, Volpp J., Kaplan A. Porosity in wire arc additive manufacturing of aluminum alloys. Additive Manufacturing 41 (2021) 101993

[17] Anyalebechi P. Hydrogen Solubility in Liquid and Solid Pure Aluminum – Critical Review of Measurement Methodologies and Reported Values. Materials Sciences and Applications 13 (2022) 158-212

[18] Valkov S., Parshorov S., Andreeva A., Rabadzhiyska S., Nikolova M., Bezdushnyi R., Petrov P. Influence of beam power on the surface architecture and corrosion behavior of electron-beam treated Co-Cr-Mo alloys. Nuclear Instruments and Methods in Physics Research B 494-495 (2021) 46-52

[19] Bhagavath S., Cai B., Atwood R., Li M., Ghaffari B., Lee P., Karagadde S. Combined Deformation and Solidification-Driven Porosity Formation in Aluminum Alloys. Metallurgical and Materials Transactions A 50 (2019) 4891-4899

[20] Chakkravarthy V., Jerome S. Fabrication of preferentially oriented Al4043 alloy and its wear anisotropy. Materials Letters 280 (2020) 128578